Research Square

An ADSCs-loaded Intelligent Delivery System Based on PLGA- PEG-PLGA Hydrogel for Promoting Anterior Cruciate Ligament Regeneration in Rabbits

Yilihamujiang Wusiman
Sixth Affiliated Hospital of Xinjiang Medical University

Xiaochen Ju
The Third Affiliated Hospital of Foshan University

Gang Chen
Sixth Affiliated Hospital of Xinjiang Medical University

Aierxiding Abulaiti
Sixth Affiliated Hospital of Xinjiang Medical University

Rongxin Sun
735242874@qq.com

Sixth Affiliated Hospital of Xinjiang Medical University

Research Article

Keywords: anterior cruciate ligament, ADSCs, PLGA-PEG-PLGA, thermosensitive hydrogel, tendon–bone healing, JNK signaling, apoptosis

Posted Date: August 5th, 2026

DOI: https://doi.org/10.21203/rs.3.rs-10327798/v1

License: This work is licensed under a Creative Commons Attribution 4.0 International License. Read Full License

Additional Declarations: No competing interests reported.

An ADSCs-loaded Intelligent Delivery System Based on PLGA-PEG-PLGA Hydrogel for Promoting Anterior Cruciate Ligament Regeneration in Rabbits

Yilihamujiang Wusiman [1], Xiaochen Ju [2], Gang Chen [1], Aierxiding Abulaiti [1], Rongxin Sun [1*];

* Corresponding author:Rongxin Sun ;Email: 735242874@qq.com;

1 Sixth Affiliated Hospital of Xinjiang Medical University , Urumqi, Xinjiang, 86830001, China.
2 The Third Affiliated Hospital of Foshan University, China.

Abstract

Background: Anterior cruciate ligament (ACL) regeneration remains challenging due to poor tendon–bone healing. Adipose-derived mesenchymal stem cells (ADSCs) combined with smart hydrogels offer a promising strategy, but their efficacy and mechanisms in ACL repair require further investigation.**Objective:** To construct a PLGA-PEG-PLGA thermosensitive hydrogel loaded with ADSCs and evaluate its ability to promote ACL regeneration in a rabbit model, focusing on cell proliferation, migration, JNK signaling, and anti-apoptotic effects. **Methods:** PLGA-PEG-PLGA copolymer was synthesized and characterized for gelation behavior, porosity, swelling, and degradation. Rabbit ADSCs were isolated, cultured, and seeded into the hydrogel. In vitro, cell adhesion, proliferation (CCK-8), migration (scratch assay), viability (live/dead staining), and JNK1 protein expression (Western blot) were assessed. In vivo, an ACL transection model was established in rabbits. The ADSCs/hydrogel composite was injected into the injury site (experimental group), while the control group received no intervention. Tendon–bone healing was evaluated at 6 and 12 weeks post-surgery using histology (HE staining), immunohistochemistry (JNK), TUNEL apoptosis assay, and biomechanical testing. **Results:** The hydrogel exhibited thermosensitive gelation at 28.5 °C, porous structure (pore diameter ~158 μm, porosity ~84.6%), and favorable swelling/degradation properties. In vitro, the hydrogel significantly promoted ADSCs proliferation (OD value at 72 h: 0.541 vs. 0.433 in control, $p < 0.05$), migration (48 h migration rate: 78.5% vs. 53.2%), and upregulated JNK1 protein expression (0.560 vs. 0.460 in control, $p < 0.05$). Cell viability remained >90% after 72 h. In vivo, the experimental group showed narrower tendon–bone interface gaps, more organized collagen fibers, higher JNK expression (68.4% vs. 42.2% at 6 weeks,$p < 0.05$), lower apoptosis index (12.4% vs. 25.7% at 6 weeks), and significantly enhanced biomechanical properties (maximum load at 12 weeks: 268.75 N vs. 182.36 N,$p < 0.05$) compared to controls.**Conclusion:** The injectable PLGA-PEG-PLGA/ADSCs hydrogel effectively promotes ACL regeneration in a rabbit model by enhancing ADSCs proliferation/migration, activating JNK signaling, and reducing local apoptosis, thereby improving tendon–bone healing and biomechanical strength.This study provides experimental evidence for a minimally invasive cell-based therapy for ACL injury.

Keywords: anterior cruciate ligament; ADSCs; PLGA-PEG-PLGA; thermosensitive hydrogel; tendon–bone healing; JNK signaling; apoptosis

Introduction

The anterior cruciate ligament (ACL) is a key stabilizer of the knee joint, primarily acting to prevent excessive forward movement of the tibia [1]. ACL tear is a common sports injury in clinical practice. The ligament has a poor intrinsic healing capacity; if not effectively treated, it often leads to knee instability, cartilage degeneration, and secondary osteoarthritis, severely impairing patients' quality of life [2–3]. Currently, arthroscopic autologous tendon graft reconstruction remains the "gold standard" for treating complete ACL ruptures [4]. However, re-tearing of the reconstructed ligament can still occur, and poor tendon–bone healing is a major contributing factor [5]. Compared with bone–bone healing, tendon–bone healing is a complex, multi-stage, and time-consuming process that generally results in inferior outcomes. Inadequate tendon–bone healing prevents patients from starting early postoperative rehabilitation, thereby compromising the surgical outcome [6–8]. Therefore, developing novel repair strategies that promote biological healing and functional regeneration of the ACL has become an important research direction in orthopedics and sports medicine.

Tissue engineering offers new possibilities for ACL repair. By combining its three core elements—scaffold materials, seed cells, and bioactive factors—it aims to mimic the natural extracellular matrix of the ligament and guide orderly tissue regeneration [9–11]. Among these, scaffold materials are crucial as they provide a temporary three-dimensional space for cell attachment, proliferation, and differentiation [12–13]. Poly(lactic-co-glycolic acid) (PLGA) has been widely used in tissue engineering because of its good biocompatibility, tunable degradation rate, and well-established processing techniques [14–15]. In particular, smart hydrogels with drug-delivery capabilities, owing to their unique injectability and in situ gelation properties, can fill irregular defect sites in a minimally invasive manner and act as an ideal vehicle for delivering cells and bioactive factors, showing great potential for clinical translation [16–17].

The choice of seed cells is another key factor for successful tissue engineering. Adipose-derived mesenchymal stem cells (ADSCs) are attractive candidates because of their abundant sources, easy accessibility, strong proliferation capacity, multi-lineage differentiation potential, and paracrine functions (including secretion of various growth factors and exosomes) [18–20]. Studies have shown that ADSCs can not only differentiate into ligament fibroblasts and directly participate in ligament matrix synthesis and remodeling, but also optimize the local injury microenvironment through potent immunomodulation and pro-angiogenic effects, thereby promoting ligament healing from multiple perspectives [21–22]. This theoretical advantage makes them superior to simple scaffold implantation or autologous tissue grafting when repairing ligament tissues with poor blood supply.

Although PLGA scaffolds and ADSCs have been extensively studied in their respective fields, research that integrates them into an injectable PLGA-based smart composite system for ACL injury repair is still at an exploratory stage, and the specific repair efficacy and underlying mechanisms remain to be systematically elucidated. Our hypothesis is that a PLGA thermosensitive hydrogel carrying ADSCs, when applied in a rabbit ACL injury model, can provide suitable physical support and biological signals, thereby effectively harnessing the tenogenic differentiation, immunomodulatory, and paracrine capabilities of ADSCs to synergistically promote structural regeneration and functional recovery of the ligament [23].

To this end, this study aimed to construct a PLGA-PEG-PLGA/ADSCs composite system and systematically evaluate its repair effect in a rabbit ACL injury model through both in vitro and in vivo experiments. We also sought to explore the potential molecular and cellular mechanisms,

focusing on promoting cell homing and proliferation, regulating macrophage polarization (M1-to-M2 transition), enhancing the orderly arrangement of collagen fibers, and facilitating angiogenesis. The hydrogel's gel-forming ability, injectability, pore size, self-healing properties, rheological behavior, as well as its degradation and swelling characteristics were evaluated. In addition, we examined temporal changes in the morphology and viability of ADSCs encapsulated in the hydrogel, along with alterations in the expression levels of tendon-bone healing-related genes and proteins, in order to inhibit degeneration and promote ACL regeneration. This study is expected to provide experimental evidence and theoretical support for developing an efficient, minimally invasive new approach for ACL repair.

1.Material Synthesis

1.1 Materials

Rabbit adipose-derived mesenchymal stem cells (ADSCs) were used in this study. The materials included PLGA biological scaffolds, DMEM/F12 culture medium, fetal bovine serum (FBS), and phosphate-buffered saline (PBS). A Cell Counting Kit-8 (CCK-8) was employed for cell proliferation assays. Primers targeting ligament-related genes, rabbit-derived anti-Col1 and anti-Col3 monoclonal antibodies, and a TUNEL apoptosis detection kit were utilized for molecular and histological analyses. Kartogenin (KGN) served as the inducing agent for ligamentogenic differentiation.

1.2 Instruments

The following instruments were used: a CO_2 incubator, a phase-contrast inverted microscope, a fluorescence microscope, and a microplate reader. Gene expression was analyzed using a real-time quantitative PCR system. Protein analysis was conducted with a Western blot electrophoresis and transfer system. Material morphology was characterized using a scanning electron microscope (SEM).

1.3 Synthesis of the PLGA-PEG-PLGA Triblock Copolymer

The thermosensitive PLGA-PEG-PLGA hydrogel was synthesized following a modified protocol based on our laboratory's established method. Briefly, the triblock copolymer was synthesized via a ring-opening polymerization reaction. Under anhydrous and oxygen-free conditions, D,L-lactide and glycolide monomers were polymerized at both termini of a poly(ethylene glycol) (PEG, Mn = 1500 Da) macroinitiator, using stannous octoate as the catalyst. The molar feed ratio of lactide (LA) to glycolide (GA) to PEG was meticulously maintained at 3:1:1, resulting in a PLGA block composition with an LA:GA ratio of 75:25. The polymerization was conducted in an oil bath at 130 °C for 24 hours.

The crude product was subsequently purified by dissolution in cold dichloromethane, followed by precipitation into an excess of ice-cold diethyl ether. This dissolution-precipitation cycle was repeated three times to ensure purity. The final polymer was obtained as a white, flocculent solid after drying to a constant weight under vacuum. The purified product was sealed and stored at -20 °C prior to use.

1.4 Preparation and Characterization of the PLGA-PEG-PLGA Hydrogel

Hydrogel Solution Preparation

A clear, free-flowing sol was prepared by dissolving the synthesized PLGA-PEG-PLGA copolymer in sterile, pre-cooled (4 °C) phosphate-buffered saline (PBS, pH 7.4) to achieve a concentration of 20% (w/v). The solution was kept at 4 °C overnight to ensure complete dissolution.

The resulting stock solution was stored on ice for subsequent use.

Thermosensitive Gelation Behavior

The sol-gel transition was assessed using the test-tube-inversion method. Briefly, 1 mL of the hydrogel solution in a vial was equilibrated at 4 °C and then transferred to a 37 °C water bath. The gelation time, defined as the time point when the flow ceased upon vial inversion, was recorded. The results are summarized in Table 1.

Morphological Observation (SEM)

The hydrogel was allowed to gel completely at 37°C, rapidly quenched with liquid nitrogen, and then lyophilized. The dried sample was sputter-coated with gold and observed under a scanning electron microscope (SEM, Hitachi SU8010) to examine its internal porous structure, as shown in Figure 1. The average pore size and porosity were subsequently analyzed from the obtained images using Image J software, with the results summarized in Table 1.

In vitroDegradation and Swelling Behavior

Pre-weighed (W_0) lyophilized hydrogel samples were immersed in PBS (containing 0.02% NaN_3 as a preservative) at 37 °C. At predetermined time points, the samples were removed, and the surface water was gently blotted with filter paper to obtain the wet weight (W_w). The samples were then re-lyophilized to determine the dry weight (W_d). The swelling ratio and remaining mass percentage were calculated using the following equations to evaluate the degradation profile: Swelling Ratio = [(W_w - W_d) / W_d] × 100%; Remaining Mass (%) = (W_d / W_0) × 100%. The degradation data are shown in Table 2.

Table1. Key physicochemical properties of the PLGA-PEG-PLGA thermosensitive hydrogel

Property	Value
Gelation time (37 °C)	45 ± 5s
Gelation temperature (Tgel)	28.5 ± 0.8 °C
Average pore diameter	158 ± 22 μm
Porosity	84.6 ± 3.2 %
Swelling ratio (24 h)	620 ± 45 %
Mass remaining (4 weeks)	58.3 ± 5.1%

Table 2. Swelling and degradation behavior of the PLGA-PEG-PLGA hydrogel over time (mean ± SD, n=3)

Time (days)	Swelling ratio (%)	Remaining mass (%)
0	100 ± 0	100 ± 0
1	485 ± 32	96.2 ± 2.1
3	612 ± 41	91.5 ± 3.0
7	638 ± 38	84.3 ± 3.5
14	590 ± 47	73.8 ± 4.2
21	520 ± 52	64.1 ± 4.8
28	445 ± 48	56.7 ± 5.0

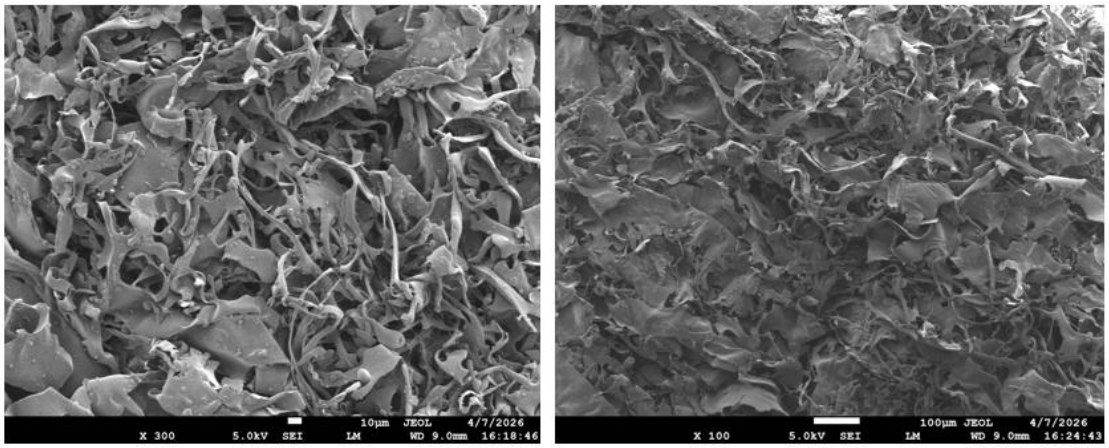


Figure 1.SEM images of the PLGA-PEG-PLGA hydrogel at 10 μm and 100 μm scales

1.5 Isolation, Culture, and Identification of ADSCs

The entire process of isolating, culturing, and passaging adipose-derived mesenchymal stem cells (ADSCs) was conducted under sterile conditions. Strict aseptic techniques were followed, and all reagents and instruments were sterilized to ensure cell viability and experimental reliability. The detailed procedures are described below.

1.5.1 Isolation of ADSCs

Subcutaneous adipose tissue was aseptically harvested from healthy adult New Zealand White rabbits weighing 2.5 ± 0.5 kg. The rabbits were anesthetized by intraperitoneal injection of 10% chloral hydrate (3 mL/kg). Subsequently, the whole body was disinfected by immersion in 75% ethanol for 10 minutes. Under a laminar flow hood, adipose tissue from the cervical or inguinal region was collected. The tissue was washed thoroughly 3-4 times with sterile PBS containing 1% penicillin-streptomycin (P/S) to remove surface blood vessels and connective tissue. The cleaned tissue was minced into approximately 1 mm^3 fragments and digested with an equal volume of 0.1-0.2% type I collagenase solution at 37°C with gentle agitation for 30-60 minutes, with manual shaking every 5-10 minutes. Digestion was terminated by adding an equal volume of complete culture medium (DMEM-LG supplemented with 10% FBS and 1% P/S). The resulting mixture was filtered through a 100 μm cell strainer to remove undigested tissue debris. The filtrate was centrifuged at 1200 rpm for 8-10 minutes. The supernatant was discarded, and the cell pellet was resuspended in complete medium to obtain the primary ADSCs suspension.

1.5.2 Primary Culture of ADSCs

The primary ADSCs suspension was centrifuged at 1200 rpm for 8-10 minutes. After discarding the supernatant, the pellet was resuspended in fresh complete medium. The cells were counted, seeded into sterile culture flasks, and incubated at 37°C in a humidified atmosphere containing 5% CO_2. The culture medium was first changed 48 hours after initial seeding, preceded by two washes with sterile PBS to remove non-adherent cells and debris. Thereafter, the medium was replaced every 2-3 days. The cells were subcultured when they reached 80-85% confluence.

1.5.3 Subculture of ADSCs

When primary ADSCs reached 80-85% confluence, they were subcultured. The old medium was aspirated, and the cell layer was rinsed twice with sterile PBS. Then, 0.25% trypsin-EDTA solution was added to cover the cell monolayer, and the flask was incubated at 37°C for 2-3 minutes. Detachment was monitored under an inverted microscope; when the cells rounded up and detached,

the digestion was stopped by adding complete medium. The cell suspension was gently pipetted to achieve a single-cell suspension, centrifuged at 1000 rpm for 8-10 minutes, and the supernatant was discarded. The cell pellet was resuspended in fresh complete medium and seeded into new culture flasks at a split ratio of 1:2 to 1:3. The cells were then returned to the incubator (37°C, 5% CO_2) for continued expansion. ADSCs at passage 3 were used for all subsequent experiments.

1.6 Construction of the Cell-Hydrogel Construct (ADSCs/PLGA Gel)

All procedures involving cell handling were performed under aseptic conditions within a laminar flow hood. Third-passage ADSCs in good growth condition were trypsinized, collected via centrifugation, and the resulting cell pellet was resuspended in a minimal volume of ice-cold complete culture medium to generate a high-density cell suspension. This concentrated cell suspension was then added dropwise, on ice, to the pre-chilled 20% PLGA-PEG-PLGA hydrogel solution. The mixture was gently pipetted to ensure homogenous cell distribution, yielding the final cell-gel composite with a cell density of 2.5×10^6 cells/mL. The composite remained in a liquid state at 4°C, making it suitable for subsequent injection applications.

2. Methods

2.1 Cell Experiments

Cell experiments were conducted to assess the adhesion, proliferation, and ligamentogenic differentiation potential of ADSCs on the PLGA scaffold, thereby evaluating the scaffold's cytocompatibility and exploring the potential mechanism by which the "PLGA scaffold + ADSCs" composite promotes ligament repair. Two experimental groups were established: the ADSCs-only group (Group A) and the PLGA scaffold-loaded ADSCs group (Group B).

2.1.2 Cell Culture and Grouping

PLGA scaffolds were cut into circular discs measuring 10 mm in diameter and 2 mm in thickness, and placed in a 24-well cell culture plate. The scaffolds were sterilized by immersion in 75% ethanol for 30 minutes, followed by five 5-minute washes with sterile PBS to remove residual ethanol. The plates were then air-dried under a laminar flow hood prior to use.

ADSCs-only group (Group A): ADSCs in the logarithmic growth phase were harvested and resuspended at a density of 1×10^5 cells/mL. A 0.5 mL aliquot of the cell suspension was seeded directly into each well of a 24-well plate. Subsequently, DMEM/F12 complete medium was added, and the cells were cultured in a 37°C, 5% CO_2 incubator.

PLGA scaffold-loaded ADSCs group (Group B): A 0.5 mL aliquot of the ADSCs suspension (1×10^5 cells/mL) was seeded onto the pre-treated PLGA scaffolds in the 24-well plate. The plate was left undisturbed for 2 hours in the incubator to allow for initial cell attachment to the scaffold surface. After this period, an additional 0.5 mL of complete medium was carefully added to each well, and the cultures were maintained under the same conditions.

2.1.3 Experimental Animals and Grouping

Forty healthy adult New Zealand White rabbits (half male and half female), weighing 2.5 ± 0.3 kg, were supplied by the Animal Laboratory of Xinjiang Medical University. All animals were acclimatized for one week under standard laboratory conditions (room temperature: 22 ± 2°C, 12-hour light/dark cycle) with free access to food and water. The experimental protocol was reviewed and approved by the Animal Ethics Committee of the Animal Laboratory at Xinjiang Medical University.

For animal model preparation and grouping, the forty rabbits were randomly assigned into two

groups using a random number table: an Injury Control group (Group A, n=20) and an Experimental group (Group B, PLGA scaffold-loaded ADSCs group, n=20).

2.2 Surgical Modeling and Intervention

2.2.1. Anesthesia and Preparation

All animals were fasted for 12 hours prior to surgery. General anesthesia was induced via intramuscular injection of Zoletil (7 mg/kg). Once anesthetized, the rabbits were positioned supine with their hind limbs secured. The surgical site was shaved and aseptically prepared with three alternating applications of povidone-iodine and 75% alcohol, followed by draping with a sterile surgical sheet.

2.2.2. Establishment of the ACL Injury Model

A medial parapatellar incision was made to access the knee joint. The skin, subcutaneous tissue, and joint capsule were incised layer by layer to fully expose the joint cavity. With the knee in a flexed position, the anterior cruciate ligament (ACL) was visualized and its midsubstance was completely transected with micro-scissors to create a complete rupture model. The joint cavity was then irrigated with sterile saline to remove any tissue debris.

2.2.3. Group Intervention

Group A (Injury Control): Following modeling, the joint capsule and skin incision were sutured layer by layer without any additional intervention.

Group B (Experimental): The ADSCs were thoroughly mixed with the pre-cooled PLGA hydrogel solution on ice to form the cell-gel composite. This composite was immediately injected into the injury site. The incision was sutured after the injected material had undergone gelation.

2.2.4. Postoperative Care

All animals received intramuscular injections of penicillin ($X\times10^4$ units/kg) for three consecutive days postoperatively to prevent infection. They were housed individually with free cage activity. Incision healing and the general condition of the animals were monitored daily.

2.3 Sample Collection

At postoperative time points of 6 and 12 weeks, a predetermined number of animals from each group were randomly selected and sacrificed by anesthetic overdose. The surgical area was dissected promptly. The tendon-bone healing complex, comprising the grafted tendon and the attached bone tissue, was carefully isolated. After removing excess surrounding soft tissue and rinsing with saline, each sample was divided into two parts: one for histological analysis (HE staining, immunohistochemistry, and TUNEL assay) and the other for biomechanical testing. Specimens designated for histological evaluation were immediately fixed in 4% paraformaldehyde. Those for biomechanical testing were preserved in ice-cold saline to prevent tissue damage that could compromise the test results.

3. Observation Indicators

3.1 Morphological Observation of ADSCs

Third-passage primary ADSCs in good growth condition were selected for observation. Culture flasks containing ADSCs were placed under an inverted microscope. After adjusting the focus, the overall cell distribution, morphological characteristics, cytoplasmic extension, and cell refractility were observed at scales of 100 μm and 50 μm. Particular attention was paid to whether the cells exhibited typical mesenchymal stem cell morphology, including the state of the cytoplasm and nucleus, the pattern of cell arrangement, and the growth density. The morphological features and

growth status were recorded to assess cell viability and determine their suitability for subsequent experiments. All cells used in this study, including those for in vivoexperiments, were third-passage primary cells.

3.2 Assessment of ADSCs Adhesion and Proliferation on PLGA Scaffolds (CCK-8 Assay)

The experiment was divided into two groups, both using passage 3 ADSCs cultured under standard conditions (37°C, 5% CO_2, humidified incubator):

1. ADSCs-only group:ADSCs were resuspended at a density of 1×10^5 cells/mL, and 0.5 mL of the suspension was seeded per well in a 24-well plate. DMEM/F12 complete medium was then added for culture.

2. PLGA scaffold-loaded ADSCs group: A 0.5 mL aliquot of the ADSCs suspension (1×10^5 cells/mL) was seeded onto pre-treated PLGA-PEG-PLGA scaffolds in a 24-well plate. The plate was left undisturbed for 2 hours to allow for cell attachment to the scaffold surface, after which an additional 0.5 mL of DMEM/F12 complete medium was added.

Cell proliferation was evaluated using the Cell Counting Kit-8 (CCK-8) assay at 0, 24, 48, and 72 hours post-seeding. At each time point, 10 μL of CCK-8 reagent was added to each well. The plate was gently shaken to ensure thorough mixing of the reagent with the culture medium, followed by incubation in the incubator for 2 hours. During incubation, the plate was protected from light, and color development was monitored periodically. After incubation, the absorbance (OD value) of each well was measured at 450 nm using a microplate reader. Each sample was measured in triplicate, and the average value was calculated. Three replicate wells were set up per group to minimize experimental error. The proliferation rate for each group was calculated based on the OD values. Subsequent statistical analysis was performed to compare differences in cell proliferation across time points and between groups, thereby clarifying the effect of the PLGA-PEG-PLGA scaffold on ADSCs adhesion and proliferation.

3.3 Cell Scratch (Wound Healing) Assay

A cell scratch assay was performed to evaluate the migratory capacity of ADSCs under different treatments. Two experimental groups were established using passage 3 ADSCs: ADSCs-only group and PLGA scaffold-loaded ADSCs group. Cell suspensions from the respective groups were seeded into 6-well plates (three replicate wells per group) and cultured in DMEM/F12 complete medium supplemented with 10% FBS and 1% P/S at 37°C, 5% CO_2 until reaching 90-100% confluence. Upon confluence, a uniform, straight scratch was created in the cell monolayer using a sterile 200 μL pipette tip, ensuring consistent scratch width across all wells to minimize human error. The wells were gently washed 2-3 times with sterile PBS to remove detached cell debris. The medium was then replaced with serum-free or low-serum (2% FBS) DMEM/F12 medium to reduce interference from growth factors during migration. The plates were returned to the incubator. Cell migration into the scratched area was observed and photographed under an inverted microscope at 0, 24, 48, and 72 hours post-scratch. Three different fields were imaged per replicate well. The scratch width at each time point was measured using ImageJ software. The cell migration rate was calculated as follows: Migration Rate (%) = [(Scratch width at 0h - Scratch width at Tx) / Scratch width at 0h] × 100%. Statistical analysis of the migration rates was conducted to determine the regulatory effect of the PLGA scaffold on ADSCs migration.

3.4 Morphological Observation of ADSCs on PLGA Scaffolds

The PLGA scaffold-loaded ADSCs group was selected for morphological observation. The

cell-scaffold constructs were examined under a phase-contrast inverted microscope at 24 and 72 hours of culture. After focusing, particular attention was paid to whether the cells successfully adhered to the PLGA-PEG-PLGA scaffold surface, as well as their morphology, spreading, pseudopodia extension, and intercellular connections. Representative images were captured (Figure 6) to provide a direct assessment of ADSCs growth status on the scaffold.

3.5 Assessment of ADSCs Viability on PLGA Scaffolds

Cell viability in the PLGA scaffold-loaded ADSCs group was assessed at 24 and 72 hours of culture using a Calcein-AM/PI Double Staining Kit, following the manufacturer's instructions. Briefly, an appropriate amount of the staining solution was added to the culture wells, followed by incubation at 37°C, 5% CO_2 for the specified duration. After incubation, the wells were observed under a fluorescence microscope. Calcein-AM penetrates live cell membranes, producing bright green fluorescence, whereas propidium iodide (PI) only enters dead cells, emitting red fluorescence. The distribution and approximate ratio of green fluorescent (live) and red fluorescent (dead) cells were recorded (Figure 7). This assessment provided an evaluation of ADSCs viability at different time points and, by extension, the cytocompatibility of the PLGA-PEG-PLGA scaffold.

3.6 Detection of JNK1 Protein Expression in ADSCs under Different Treatments

Three experimental groups were established for protein analysis: ADSCs-only group, PLGA scaffold-loaded ADSCs group, and a KGN-treated group (positive control for ligamentogenic differentiation), all using passage 3 ADSCs. After culture under respective conditions, ADSCs from each group were collected. Total protein was extracted using RIPA lysis buffer supplemented with protease inhibitors. The lysates were centrifuged at 4°C, and the supernatant was collected. Protein concentration was determined using the BCA assay and normalized to ensure equal loading. Proteins were separated by SDS-PAGE and transferred onto PVDF membranes. The membranes were blocked with 5% skim milk at room temperature for 1.5-2 hours to prevent nonspecific binding. After blocking, the membranes were incubated with the primary antibody against JNK1 at 4°C overnight. The following day, the membranes were washed three times (10 min each) with TBST buffer and then incubated with the corresponding secondary antibody at room temperature for 1 hour, followed by another three TBST washes. Protein bands were visualized using a chemiluminescence method and imaged with a gel documentation system (Figure 8). The grayscale values of the JNK1 bands were quantified using ImageJ software. β-actin served as the loading control for calculating the relative expression level of JNK1 protein in each group. Experiments were performed with three biological replicates, and statistical analysis was conducted to compare differences in JNK1 protein expression among groups, exploring the potential molecular mechanisms by which the PLGA-PEG-PLGA scaffold influences ligament repair.

4. Animal Experiments

4.1 Hematoxylin and Eosin (H&E) Staining

The fixed tendon-bone specimens were processed through a graded ethanol series (70%, 80%, 90%, 95%, and 100%) for dehydration, cleared in xylene, and embedded in paraffin. Serial sections of 5 μm thickness were obtained. The sections were deparaffinized and rehydrated (xylene, twice for 10 min each; descending ethanol series from 100% to 70%, 5 min each; rinsed twice with distilled water). Staining was performed with hematoxylin for 5-10 minutes, followed by rinsing with tap water to remove excess dye. Differentiation was carried out in 1% acid alcohol for 30 seconds, and the sections were blued in tap water for 10 minutes. Counterstaining was done with

eosin for 30 seconds. Finally, the sections were dehydrated through a graded alcohol series, cleared in xylene, and mounted with neutral resin. The morphology of the tendon-bone interface, collagen fiber formation, and cell infiltration were observed under a light microscope. Photomicrographs were captured (see Figure 9), with a focus on analyzing the gap at the tendon-bone interface, the arrangement of collagen fibers, and the bonding tightness between groups at different time points.

4.2 Immunohistochemical Staining for JNK Protein

Expression of JNK protein in the tendon-bone healing tissue was detected using the streptavidin-peroxidase (SP) immunohistochemical method. Paraffin sections of the tendon-bone specimens were deparaffinized and rehydrated. Endogenous peroxidase activity was quenched by incubating the sections with 3% H_2O_2 at room temperature for 10 minutes. After rinsing with distilled water, the sections were washed three times with PBS (5 min each). Antigen retrieval was performed using citrate buffer with microwave heating for 10 minutes. After cooling to room temperature, the sections were washed three times with PBS. Non-specific binding sites were blocked with 5% goat serum at room temperature for 30 minutes. The blocking solution was removed without washing. The sections were then incubated with the primary antibody against JNK (diluted 1:100) at 4°C overnight. The following day, after three 5-minute PBS washes, the corresponding secondary antibody was applied and incubated at room temperature for 1 hour, followed by another three PBS washes. Color development was performed using DAB substrate, with the reaction time (3-5 minutes) controlled under microscopic observation. The reaction was stopped by rinsing with distilled water. The nuclei were lightly counterstained with hematoxylin for 30 seconds, blued in tap water, and then the sections were dehydrated, cleared, and mounted. Positive signals appeared as brownish-yellow staining. Five random high-power fields (×400 magnification) were selected for each section. The percentage of positive cells was counted to calculate the JNK protein-positive expression rate. Photomicrographs were taken (see Figures 10 & 11) for subsequent statistical analysis.

4.3 Biomechanical Testing

Tendon-bone specimens (the graft tendon-bone tissue complex) collected at 6 and 12 weeks postoperatively were mounted on a biomechanical testing machine. A tensile test was performed at a constant speed (e.g., 1 mm/min). The tendon and bone ends were firmly and uniformly fixed to the clamps to prevent slippage or eccentric failure. The test machine was activated to apply uniaxial tension until specimen failure. The maximum load (the peak force at failure) and the maximum displacement (the elongation at break) were recorded. Several specimens from each group at each time point were tested. The average values were calculated and subjected to statistical analysis to compare the differences in biomechanical properties between groups at different time points.

4.4 Statistical Analysis

Statistical analysis was performed using SPSS software (version 27.0). Measurement data were first tested for normality. Data conforming to a normal distribution are presented as the mean ± standard deviation ($\bar{x} \pm s$). One-way analysis of variance (One-way ANOVA) was used for comparisons among groups. The SNK-q test was employed for post-hoc pairwise comparisons. A significance level of $\alpha = 0.05$ was set, and a P-value < 0.05 was considered statistically significant. The entire statistical process was completed using SPSS 27.0.

5. Results

5.1 Morphological Observation of ADSCs

The morphological characteristics of adipose-derived mesenchymal stem cells (ADSCs) observed under an inverted microscope are shown in Figure 2 . The results revealed that the ADSCs exhibited a typical elongated, spindle-shaped morphology. The cells possessed abundant and plump cytoplasm with clear, centrally located nuclei. They were distributed loosely and uniformly, displaying a consistent morphology and growing in a disordered or slightly swirling pattern, which aligns with the typical characteristics of ADSCs. Third-passage primary ADSCs were used for all in vitro and in vivo experiments. At a scale of 100 μm, the cells were evenly distributed without significant aggregation, indicating good growth status. At a higher magnification (50 μm scale), the spindle shape of the cells was clearly distinguishable. The cell bodies were fully extended with slender and distinct pseudopodia, and the cells showed strong refractility, suggesting high viability and suitability for subsequent experiments.

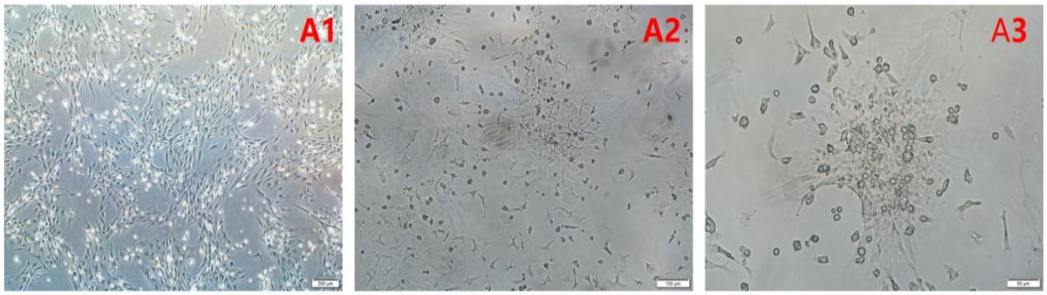


Figure 2 Morphological observation of ADSCs

5.2 Adhesion and Proliferation of ADSCs on PLGA Scaffolds (CCK-8 Assay)

The CCK-8 assay results for the proliferation activity of ADSCs in the two groups are shown in Table 3. The proliferative activity of ADSCs in both groups showed an increasing trend over time, with significant differences observed between groups. At 0 hours, there was no significant statistical difference in the OD values between the two groups ($P > 0.05$), indicating consistent initial cell seeding and a uniform experimental baseline. The OD values for both groups at 24, 48, and 72 hours were significantly higher than those at the previous time point ($P < 0.05$), demonstrating a clear time-dependent proliferative characteristic. Specifically, the OD values for the PLGA scaffold-loaded ADSCs group were higher than those of the ADSCs-only group at all time points. Detailed OD values are presented in Table 3. Statistical analysis indicated that the OD values for the PLGA scaffold-loaded ADSCs group at 48 and 72 hours were significantly higher than those of the ADSCs-only group at the corresponding time points ($P < 0.05$). These results suggest that the PLGA-PEG-PLGA scaffold provides a favorable three-dimensional microenvironment for ADSCs adhesion and proliferation, significantly promoting cell growth without exhibiting apparent cytotoxicity.

Table 3 CCK8 assay data ($\bar{x} \pm s$)

Index	Time Point	ADSCs Group	PLGA Scaffold-Loaded ADSCs Group	F Value	P Value
OD Value	0 h	0.188±0.012	0.180±0.010	0.76	＞0.05
	24 h	0.249±0.016	0.304±0.018	4.21	＜0.01
	48 h	0.351±0.019	0.432±0.021	5.67	＜0.01
	72 h	0.433±0.021	0.541±0.023	7.13	＜0.01

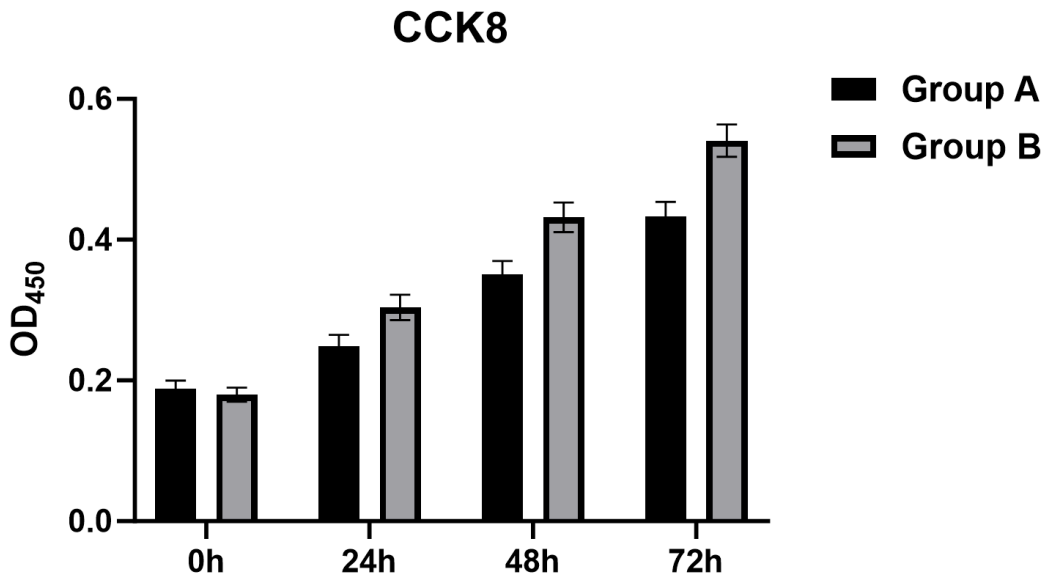


Figure 3 Bar chart analysis of the CCK8 assay

5.3 Cell Scratch Assay Results

The results of the cell scratch assay, assessing the migratory capacity of ADSCs in the two groups, showed that cell migration ability gradually increased with culture time after scratching, and distinct differences were observed between groups. At 0 hours post-scratch, the scratch widths were consistent between the two groups with no statistical difference ($P > 0.05$). At 24 and 48 hours post-scratch, the scratch width in the PLGA scaffold-loaded ADSCs group was significantly narrower than in the ADSCs-only group ($P < 0.05$). At 72 hours, the difference remained significant ($P < 0.05$).

The calculated cell migration rates showed that the PLGA scaffold-loaded ADSCs group had significantly higher migration rates at 24, 48, and 72 hours compared to the ADSCs-only group ($P < 0.05$), and the rate increased over time. At 24 hours, the migration rate was (42.36 ± 3.85)% for the PLGA scaffold-loaded ADSCs group and (28.15 ± 3.12)% for the ADSCs-only group. By 48 hours, the migration rate in the PLGA scaffold-loaded ADSCs group increased to (78.52 ± 4.13)%, while the rate for the ADSCs-only group was (53.24 ± 3.96)%. At 72 hours, the migration rates were (89.34 ± 3.87)% and (65.42 ± 4.01)%, respectively. These results indicate that the PLGA-PEG-PLGA scaffold can significantly enhance the migratory capacity of ADSCs, potentially increasing their potential to migrate towards injury sites.

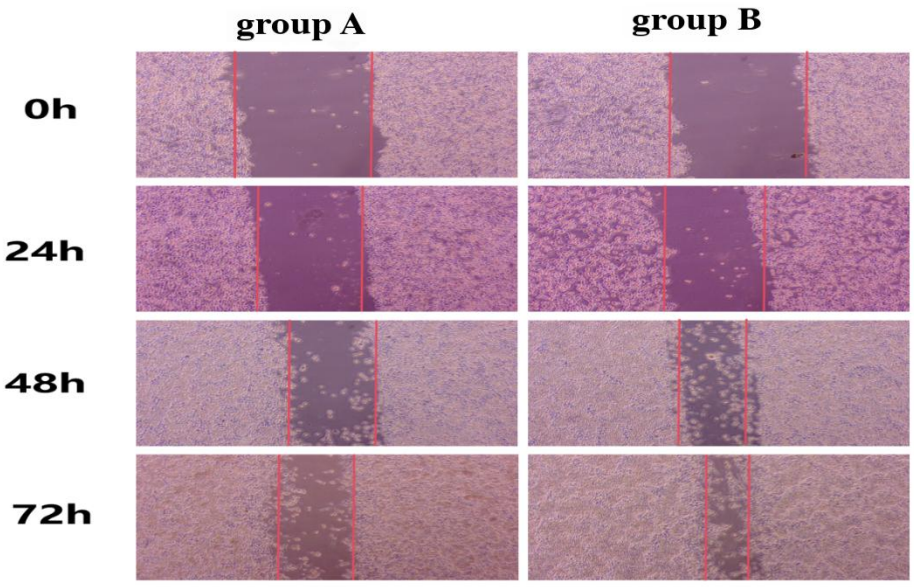


Figure 4 Scratch assay of ADSCs

Table 4 Results of the cell scratch assay μ m ($\bar{x} \pm s$)

Index	Time Point	ADSCs Group (μm)	PLGA Scaffold-Loaded ADSCs Group (μm)	F Value	P Value
Scratch Width	0 h	465.3 ± 20.1	466.0 ± 18.5	0.01	> 0.05
	24 h	358.6 ± 15.2	312.4 ± 14.8	7.92	< 0.05
	48 h	298.5 ± 12.4	235.6 ± 11.3	14.86	< 0.05
	72 h	210.3 ± 18.6	135.8 ± 12.7	17.33	< 0.05

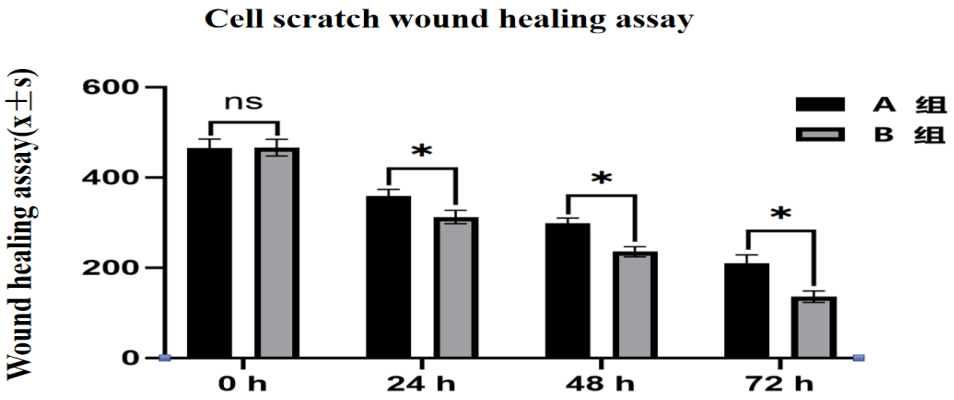


Figure 5 Bar chart of the cell scratch assay

5.4 Morphological Observation of ADSCs on PLGA Scaffolds

Dynamic observation of cell morphology in the PLGA scaffold-loaded ADSCs group under a phase-contrast inverted microscope (see Figure 6) revealed that after 24 hours of culture, ADSCs had successfully adhered to the PLGA-PEG-PLGA scaffold surface. The cells displayed a typical spindle shape, began to spread, and formed initial pseudopodia, with a small number starting to

connect with each other. By 72 hours, the cell number had increased significantly. The cells were fully spread across the scaffold surface and within its pores, exhibiting well-extended cell bodies with slender and developed pseudopodia. The cells were interconnected, forming a dense cellular layer with a plump morphology and healthy growth status. These observations visually demonstrate that the PLGA-PEG-PLGA scaffold possesses good cell adhesiveness, supports normal ADSCs growth and spreading, and provides a stable microenvironment for the cells.

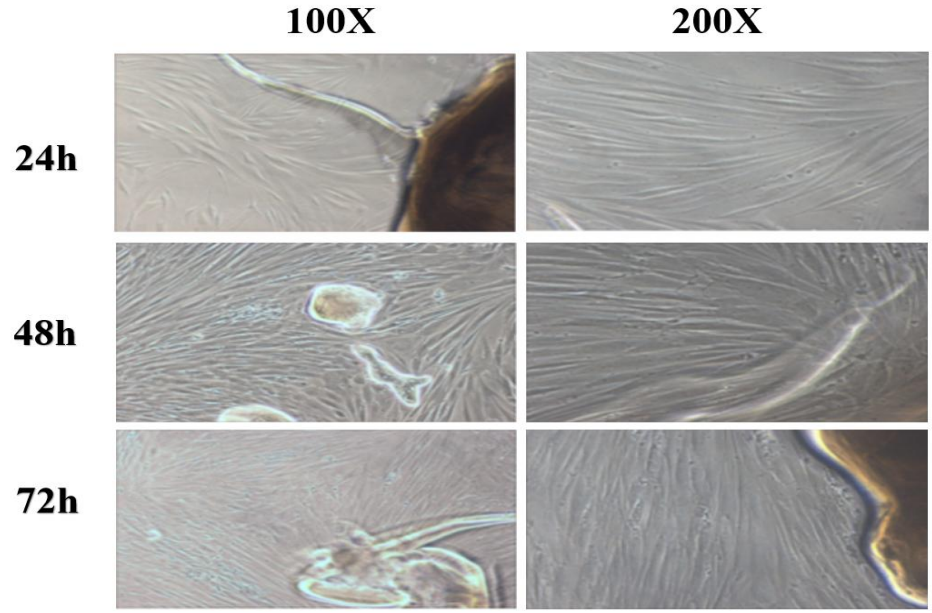


Figure 6 Microscopic view of rabbit ADSCs

5.5 Viability of ADSCs on PLGA Scaffolds

The viability of ADSCs in the PLGA scaffold-loaded ADSCs group, assessed by Calcein-AM/PI double staining (see Figure 7), showed that after 24 hours of culture, the visual field was dominated by bright green fluorescence (live cells stained with Calcein-AM), with very few red fluorescent spots (dead cells stained with PI). The cell viability rate was over 95%, indicating excellent survival status of ADSCs after adhesion to the scaffold. After 72 hours, green fluorescence still predominated, with most cells remaining viable and only sporadic red fluorescent dots observed. The cell viability rate remained above 90%, suggesting that although a small number of cells underwent natural death over time, the overall survival status remained favorable. In summary, the PLGA-PEG-PLGA scaffold exhibits good cytocompatibility, maintaining a high viability rate of ADSCs over an extended period, thereby supporting cell growth, proliferation, and function.

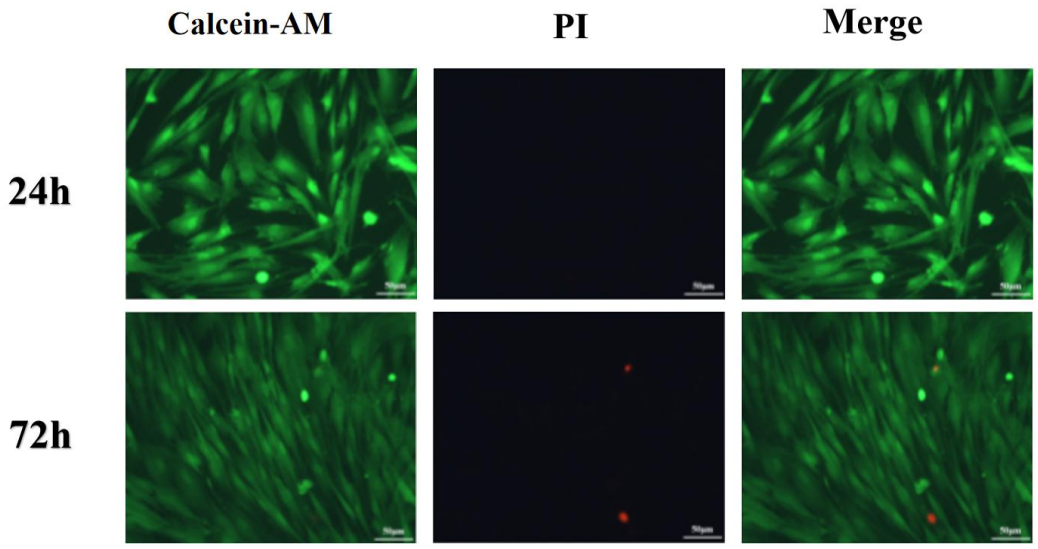


Figure 7 Calcein-AM/propidium iodide (PI) staining

5.6 Effect of Different Treatments on JNK1 Protein Expression in ADSCs

Western Blot analysis of JNK1 protein expression levels in ADSCs from the three groups (see Figure 8and Table 5) revealed significant differences in the relative expression levels among the groups ($P < 0.05$). The PLGA scaffold-loaded ADSCs group showed the highest relative expression of JNK1 protein (0.560 ± 0.088). The relative expression in the ADSCs-only group (0.460 ± 0.060) was intermediate between the PLGA scaffold group and the KGN-treated group (positive control for ligamentogenic differentiation), which had the lowest expression (0.397 ± 0.039). Statistical analysis indicated that the JNK1 protein expression level in the PLGA scaffold-loaded ADSCs group was significantly higher than that in the KGN-treated group ($P < 0.05$), while no significant difference was found between the ADSCs-only group and the KGN-treated group ($P > 0.05$). These results suggest that the microenvironment provided by the PLGA-PEG-PLGA scaffold can significantly upregulate the expression of JNK1 protein, a key component of the JNK signaling pathway, in ADSCs. This upregulation may represent one of the potential molecular mechanisms through which the scaffold promotes ligament repair.

Table 5. Comparison of relative JNK1 protein expression in ADSCs among different treatment groups (mean ± SD, n=3)

Group	Relative JNK1 Protein Expression (mean ± SD, n=3)
ADSCs	0.460±0.060
PLGA/ADSCs	0.560±0.088*
KGN	0.397±0.039
Note: *P < 0.05 compared with the KGN-treated group	

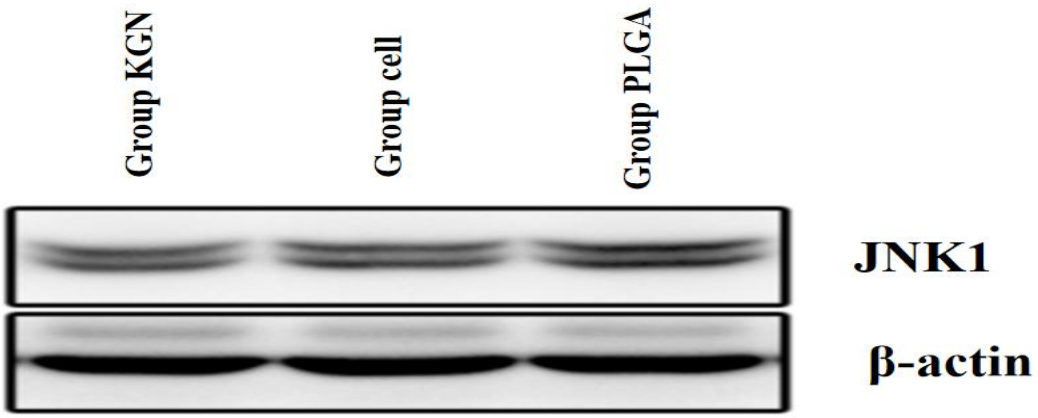


Figure 8 Western blot bands

5.7 Animal Experimental Results

A total of eight animals were excluded from the study due to incision infection: two from the control group and three from the experimental group. Another seven animals died: four in the control group and three in the experimental group. Consequently, twenty-eight animals completed the study, comprising 12 in the control group and 16 in the experimental group. The included animals exhibited good mental status and normal food intake postoperatively. All surgical incisions healed properly without complications such as re-infection or suture dehiscence. No additional deaths occurred during the housing period, confirming their suitability for the experimental analysis.

5.7.1 H&E Staining Observations

At 6 weeks post-operation, the control group exhibited a distinct gap at the tendon-bone interface. Collagen fibers were disorganized and sparse, with only minimal cell infiltration and no apparent formation of mature collagen fibers, resulting in a loose tendon-bone connection. In contrast, the experimental group showed a markedly reduced interface gap. Collagen fibers were more regularly aligned, cell infiltration was increased, and the early formation of some mature collagen fibers was observed, leading to a tighter tendon-bone integration.

By 12 weeks, although the interface gap in the control group had diminished somewhat, a clear boundary remained. Collagen fiber alignment was still disordered, and the amount of mature collagen was limited. The experimental group, however, demonstrated near-complete obliteration of the interface gap. Collagen fibers were densely and regularly arranged, forming substantial mature collagen, which facilitated a tight, continuous tendon-bone integration (see Figure 9).

Statistical analysis confirmed that the maturity of collagen fibers and the tightness of the tendon-bone interface in the experimental group were significantly superior to those in the control group at both 6 and 12 weeks ($P < 0.05$).

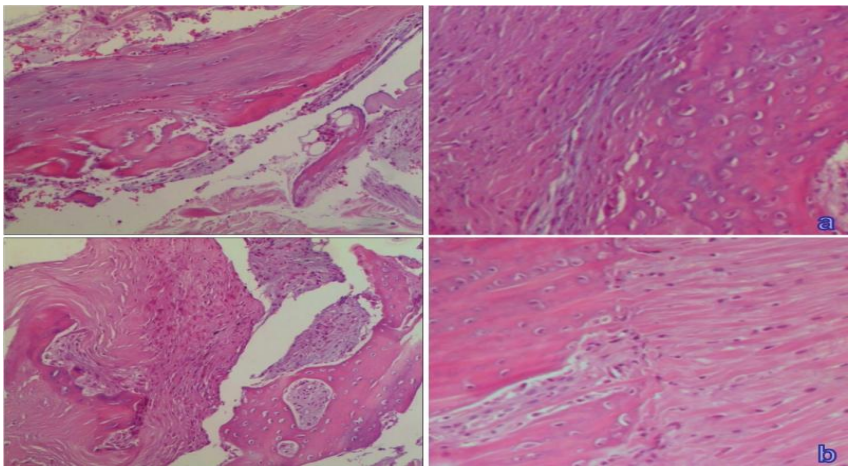


Figure 9. H&E staining observation of the tendon-bone interface in each group.
Specimens from groups A to B are shown from left to right. The gap between the grafted tendon and bone tissue is indicated by arrows. B: bone tissue; T: grafted tendon. a. 6 weeks post-operation; b. 12 weeks post-operation.

5.7.2 Immunohistochemical Staining for JNK Protein

The expression of JNK protein in the tendon-bone healing tissue, detected by the streptavidin-peroxidase (SP) immunohistochemical method, is shown in Figure 10. Positive JNK signals, appearing as brownish-yellow staining, were localized primarily in the cytoplasm and nuclei of cells at the tendon-bone interface. At 6 weeks post-operation, the positive expression rate of JNK protein in the experimental group was 68.35 ± 4.21%, significantly higher than the 42.18 ± 3.95% in the control group ($P < 0.05$). At 12 weeks, the positive rate in the experimental group (52.47 ± 3.86%) remained significantly elevated compared to the control group (31.69 ± 3.58%) ($P < 0.05$). While the JNK-positive expression rates in both groups showed a decreasing trend over time, the rates in the experimental group were consistently and significantly higher than those in the control group at each time point. This suggests that the intervention combining the PLGA-PEG-PLGA scaffold with ADSCs can significantly upregulate JNK protein expression in the healing tissue, implicating its involvement in the tendon-bone healing process.

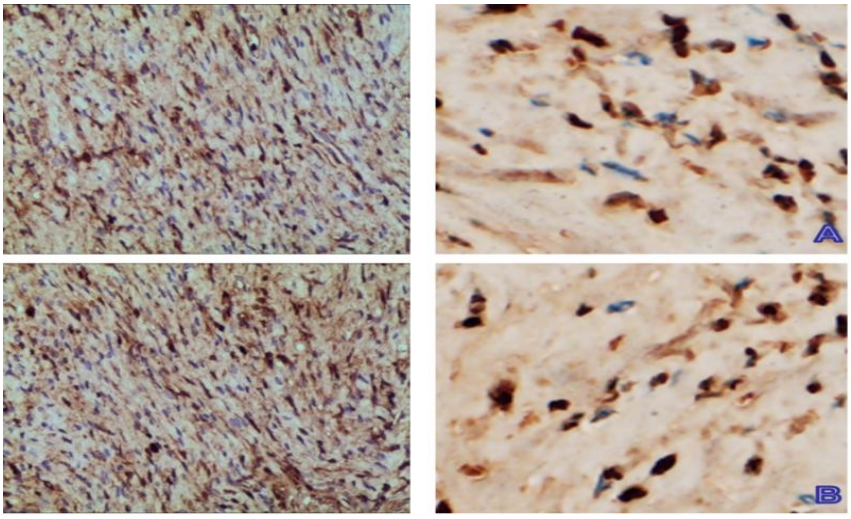


Figure 10. Expression of JNK protein.
The images from left to right represent the 6-week and 12-week time points, respectively. A:

Control group; B: Experimental group.

5.7.3 TUNEL Apoptosis Assay Results

The TUNEL apoptosis assay results showed apoptotic cell nuclei stained brown/black (appearing as blue fluorescence under DAPI counterstain), while normal cell nuclei were blue. The apoptotic index (AI) in the experimental group at 6 weeks was 12.35 ± 1.86%, significantly lower than the 25.68 ± 2.34% in the control group ($P < 0.05$). At 12 weeks, the AI in the experimental group (8.42 ± 1.53%) remained significantly lower than that in the control group (18.75 ± 2.11%) ($P < 0.05$). The apoptotic index decreased over time in both groups. However, the experimental group exhibited a consistently and significantly lower AI than the control group at all time points. This indicates that the combined intervention of the PLGA-PEG-PLGA scaffold and ADSCs significantly inhibits cell apoptosis in the tendon-bone healing tissue, reducing cell death and thereby providing a more favorable cellular foundation for healing.

5.7.4 JNK Immunohistochemical Staining (Additional Observations)

JNK immunohistochemical staining revealed brownish-yellow nuclei in all groups at 6 weeks, with the staining intensity gradually decreasing by 12 weeks. At both time points, Group B (experimental group) displayed the deepest staining intensity (Figure 11). Statistically, the positive expression rate of JNK protein in Group B was significantly higher than in Group A (control) at both 6 and 12 weeks post-operation ($P < 0.05$). Furthermore, the JNK positive expression rates in both Group A and Group B at 12 weeks were significantly lower than their respective rates at 6 weeks ($P < 0.05$).

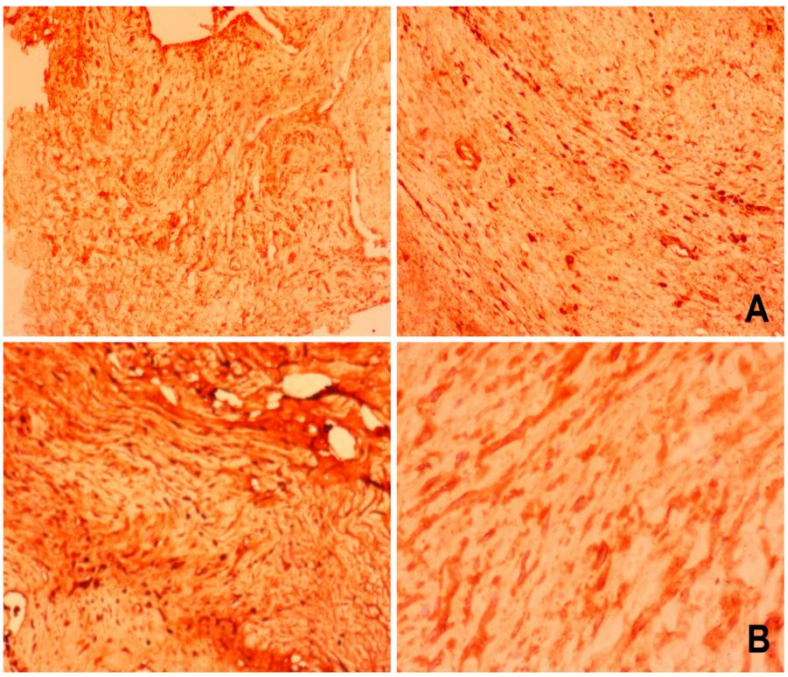


Figure 11 Immunohistochemical staining of JNK in each group (6 weeks and 12 weeks, from left to right; Group A: control group, Group B: experimental group)

5.7.5 Biomechanical Testing Results

The biomechanical tensile testing results demonstrated that the maximum load and the maximum displacement at failure of the tendon-bone complexes in both groups increased significantly over time ($P < 0.05$). Crucially, the biomechanical properties of the experimental group

were significantly superior to those of the control group at each postoperative time point ($P < 0.05$). Specific data are detailed in Table 6.

Table 6. Comparison of biomechanical test results between the two groups at different postoperative time points (mean ± SD)

Postoperative Time	Group	Maximum Load (N) (mean ± SD)	Maximum Displacement (mm) (mean ± SD)
6 weeks	Control	128.45±12.67	2.18±0.35
6 weeks	Experimental	185.62±15.34*	3.25±0.42*
12 weeks	Control	182.36±14.89	3.05±0.48
12 weeks	Experimental	268.75±18.46*	4.52±0.51*

Note: *$P < 0.05$ compared with the control group at the same time point. Intergroup difference: $F = 10.256$, $P = 0.001$. Intragroup time effect: $F = 12.873$, $P = 0.000$.

6 Discussion

1. PLGA-PEG-PLGA Hydrogel Provides a Favorable Microenvironment for ADSCs

The successful application of stem cell-based tissue engineering heavily relies on the scaffold's ability to support cell survival, adhesion, and function [24]. The PLGA-PEG-PLGA hydrogel we synthesized possesses a porous structure (pore size: 100–300 μm), suitable swelling and degradation behavior, and thermosensitive gelation at 37 °C, enabling minimally invasive injection and in situ scaffold formation.

CCK-8 assays revealed that ADSCs cultured on the hydrogel exhibited significantly higher proliferation rates at 48 and 72 hours compared to ADSCs in monolayer culture ($P < 0.05$). This enhanced proliferation was further corroborated by live/dead staining, which showed a cell viability exceeding 90% after 72 hours of culture, indicating excellent cytocompatibility.

Furthermore, the scratch wound assay demonstrated that the hydrogel promoted ADSCs migration, with a migration rate of 78.5% at 48 hours versus 53.2% in the control group ($P < 0.05$). Improved cell adhesion and spreading, as observed by phase-contrast microscopy, supports the notion that the surface topography and porous architecture of the hydrogel are conducive to favorable cell-scaffold interactions.

2. Enhanced In VivoTendon-Bone Healing and Biomechanical Performance

In the rabbit ACL injury model, the experimental group (PLGA-PEG-PLGA + ADSCs) demonstrated a significantly narrower tendon-bone interface gap, more ordered collagen fiber alignment, and higher mature collagen content at both 6 and 12 weeks post-operation compared to the control group (injury only).

By 12 weeks, the experimental group achieved near-continuous integration at the tendon-bone interface, whereas a discernible gap persisted in the control group. Histologically, this improved healing was accompanied by increased cell infiltration and active extracellular matrix remodeling.

Biomechanically, the maximum failure load and maximum displacement at failure for the

experimental group were significantly higher than those of the control group at both time points (e.g., at 12 weeks: 268.75 N vs. 182.36 N, $P < 0.05$). The strong correlation between histological organization and mechanical strength suggests that the hydrogel-ADSCs construct not only accelerates early healing but also promotes long-term functional recovery.

3. Mechanism Exploration: JNK Activation and Anti-Apoptotic Effect

A key finding of this study is that the ADSCs-laden hydrogel upregulated JNK1 protein expression in ADSCs in vitroand enhanced JNK protein expression in the tendon-bone healing tissue in vivo.

Western blot analysis indicated that the relative expression of JNK1 in ADSCs cultured on the hydrogel was 0.560 ± 0.088, significantly higher than that in the KGN-treated group (0.397 ± 0.039, $P < 0.05$). Immunohistochemistry further confirmed that the percentage of JNK-positive cells in the experimental group was higher than in the control group at both 6 weeks (68.4% vs. 42.2%) and 12 weeks (52.5% vs. 31.7%) post-operation ($P < 0.05$).

The JNK signaling pathway plays a dual role in tissue repair, mediating inflammatory responses but also promoting cell proliferation, migration, and ligamentogenic differentiation under appropriate conditions [25]. In ligament healing, JNK activation has been associated with improved fibroblast function and enhanced collagen synthesis [26]. Our data suggest that the PLGA-PEG-PLGA hydrogel may create a mechano-biological microenvironment that potentiates JNK signaling in ADSCs, thereby promoting their differentiation toward ligament fibroblasts. However, it should be noted that we only measured total JNK1. Future studies should investigate phosphorylated JNK (p-JNK) and its downstream effectors (e.g., c-Jun, AP-1) to confirm pathway activation.

Additionally, TUNEL assays revealed significantly lower apoptotic indices in the experimental group at both 6 and 12 weeks (6 weeks: 12.4% vs. 25.7%, $P < 0.05$). This anti-apoptotic effect may be attributed to paracrine factors secreted by ADSCs, including VEGF, HGF, and exosomes, which have been shown to protect local cells from ischemia-induced death [27, 28]. Reduced apoptosis likely helps maintain cellularity at the tendon-bone interface, further facilitating matrix remodeling.

4. Limitations

Several limitations of this study should be acknowledged. First, the animal model involved complete transection of the rabbit ACL, which does not fully replicate the clinical scenarios of chronic degeneration or partial tears. Second, the absence of a hydrogel-only control group precludes a clear distinction between the individual contributions of the hydrogel scaffold and the ADSCs. Third, the mechanistic analysis was limited to JNK1; upstream regulators (e.g., integrin signaling) and downstream transcription factors were not explored. Finally, outcomes beyond 12 weeks were not evaluated, and potential risks such as ectopic tissue formation or immune responses were not systematically examined.

5. Conclusion

In summary, this study demonstrates that an injectable, thermosensitive PLGA-PEG-PLGA hydrogel loaded with ADSCs effectively promotes ACL regeneration in a rabbit model. The composite system enhanced ADSCs proliferation, migration, and viability, improved tendon-bone interface healing, and increased biomechanical strength. The underlying mechanisms may involve activation of the JNK signaling pathway and suppression of local cell apoptosis.

Despite the aforementioned limitations, this work provides a solid experimental foundation for developing a minimally invasive, cell-based therapy for ACL injuries. Future research should focus on optimizing the hydrogel's degradation kinetics to match the ligament remodeling process,

exploring the role of ADSCs-derived exosomes, and evaluating long-term functional outcomes in large animal models.

Conflict of Interest: All authors of the article declare that there is no conflict of interest in the research and writing of the article.

Biostatistics Statement: The statistical methods in this paper have been reviewed by biostatistics experts from Xinjiang Medical University.

Availability of data and materials: Data sets used and/or analyzed during the current study period may be obtained from the corresponding author upon reasonable request.

Clinical trial number: not applicable.

Fund Information: Rongxin Sun, Tianshan Talents Program for Medical and Health Leading Professionals, Health Commission of the Xinjiang Uygur Autonomous Region, TSYC202301A034

References

[1] Filbay, S. R., Bullock, G., Russell, S., Brown, F., Hui, W., & Egerton, T. (2025). No Difference in Return-to-Sport Rate or Activity Level in People with Anterior Cruciate Ligament (ACL) Injury Managed with ACL Reconstruction or Rehabilitation Alone: A Systematic Review and Meta-Analysis: SR Filbay et al. *Sports Medicine*, *55*(9), 2191-2205.

[2] Yeo, I. S., Hong, J. E., & Yang, H. M. (2025). Histomorphometric analysis of anterior cruciate ligament bundles and anatomical insights into injury mechanisms. *Scientific reports*, *15*(1), 6762.

[3] Gao, Z., Xiang, L., Jiang, H., Mei, Q., Fekete, G., Baker, J. S., & Gu, Y. (2025). Musculoskeletal modelling sequentially integrated with stress simulation reveals asymmetrical knee loading and ligament stress during long-distance running. BMC Sports Science, Medicine and Rehabilitation, 17(1), 337.

[4] Kittani, M., Haviv, B., Shemesh, S., Yaari, L., Yassin, M., & Rath-Wolfson, L. (2021). Morphological and Histological Changes in the Human Anterior Cruciate Ligament after Rupture. *The Israel Medical Association Journal: IMAJ*, *23*(1), 33-37.

[5] Zhu, Y., Sun, H., Wang, X., Li, J., & Fu, W. (2026). Comparison of Knee Function After Reconstruction With Posterolateral Corner Injury and With or Without Posteromedial Corner Injury for Treating Knee Dislocation Cases: A Prospective Cohort Study. Orthopaedic Surgery, 18(4), 721-732.

[6] Jiang, F., Zhao, H., Zhang, P., Bi, Y., Zhang, H., Sun, S., ... & Xiao, X. (2024). Challenges in tendon–bone healing: emphasizing inflammatory modulation mechanisms and treatment. *Frontiers in Endocrinology*, *15*, 1485876.

[7] Yang, C., Teng, Y., Geng, B., Xiao, H., Chen, C., Chen, R., ... & Xia, Y. (2023). Strategies for promoting tendon-bone healing: current status and prospects. *Frontiers in bioengineering and*

biotechnology, *11*, 1118468.

[8] Li, H., Li, Z. P., Zhu, M. T., Lan, C. H., Wang, Y. X., Liao, P., ... & Xu, G. H. (2025). Optimizing mesenchymal stem cell therapy for tendon-bone healing: Multifaceted approaches and future directions. World Journal of Stem Cells, 17(12), 114076.

[9] Simon, F., Caneparo, C., Moreira-Pereira, J., & Chabaud, S. (2026). Anterior Cruciate Ligament Tissue Engineering: Biological Principles, Engineered Substitutes, and Preclinical Outcomes. *Bioengineering*, *13*(4), 442.

[10] Yu, C., Chen, R., Chen, J., Wang, T., Wang, Y., Zhang, X., ... & Yu, T. (2024). Enhancing tendon-bone integration and healing with advanced multi-layer nanofiber-reinforced 3D scaffolds for acellular tendon complexes. Materials Today Bio, 26, 101099.

[11] Shen, S., Lin, Y., Sun, J., Liu, Y., Chen, Y., & Lu, J. (2024). A New Tissue Engineering Strategy to Promote Tendon–bone Healing: Regulation of Osteogenic and Chondrogenic Differentiation of Tendon-derived Stem Cells. Orthopaedic Surgery, 16(10), 2311-2325.

[12] Kadyr, S., Nurmanova, U., Khumyrzakh, B., Zhakypbekova, A., Saginova, D., Daniyeva, N., & Erisken, C. (2024). Braided biomimetic PCL grafts for anterior cruciate ligament repair and regeneration. Biomedical Materials, 19(2), 025034.

[13] Yu, C., Feng, S., Li, Y., & Chen, J. (2023). Application of nondegradable synthetic materials for tendon and ligament injury. Macromolecular Bioscience, 23(12), 2300259.

[14] Zhang, H., Chen, X., Ong, M. T. Y., Lei, L., Zheng, L., Dai, B., ... & Qin, L. (2025). Current advances of artificial ligaments for anterior cruciate ligament reconstruction: from biocompatibility to bioactivity. *Engineering*, *46*, 47-59.

[15] Ren, Y., Chen, B., & Li, A. (2021). Research and exploration of ACL injury repair and reconstruction and application of biomaterials. *International Journal of Nanotechnology*, *18*(1-4), 226-239.

[16] Meng, Q., Zhang, N., Xiao, M., Zhou, L., Leng, H., & Bao, C. (2025). Hydrogel-based treatment of ACL injuries: mechanisms, applications and prospects. *European Polymer Journal*, 114222.

[17] Zhang, M., Feng, Q., Zhang, G., Wang, R., Zhang, H., Li, M., ... & Nie, Y. (2025). Calcium-capturing hydrogel with self-reinforced multi-dynamic networks for effective periodontal bone regeneration in three-dimension. Advanced Functional Materials, 35(12), 2415185.

[18] Li, H., Li, Z. P., Zhu, M. T., Lan, C. H., Wang, Y. X., Liao, P., ... & Xu, G. H. (2025). Optimizing mesenchymal stem cell therapy for tendon-bone healing: Multifaceted approaches and future directions. World Journal of Stem Cells, 17(12), 114076.

[19] Wu, Y., Wang, X., Zhao, D., Lin, R., Zhang, X., & Lin, X. (2025). Tendon–Bone Healing: Synergistic Role of Platelets and Mesenchymal Stem Cells in Tissue Engineering. Tissue

Engineering Part B: Reviews.

[20] Huang, C., Lu, G., Jia, Z., & Yan, J. (2025). Mesenchymal Stem Cell–Derived Exosome miR-153–3 Induced M2-Type Polarization of Macrophages to Improve the Healing Effect of Burn Wounds. Applied biochemistry and biotechnology, 197(6), 3841-3855.

[21] Neculachi, C. A., Nastase-Rusu, E. G., Cherry, L., Marinescu-Colan, C. I., Tastsoglou, S., Cosman, B. P., ... & Burlacu, A. (2025). miR-210 promotes the anti-inflammatory phenotype and M2 polarization in murine macrophages. Frontiers in immunology, 16, 1633163.

[22] Fu, X., Liu, G., Halim, A., Ju, Y., Luo, Q., & Song, G. (2019). Mesenchymal stem cell migration and tissue repair. Cells, 8(8), 784.

[23] He, X., Li, Y., Guo, J., Xu, J., Zu, H., Huang, L., ... & Qin, L. (2021). Biomaterials developed for facilitating healing outcome after anterior cruciate ligament reconstruction: efficacy, surgical protocols, and assessments using preclinical animal models. Biomaterials, 269, 120625.

[24] Higa, K., Murata, D., Azuma, C., Nishida, K., & Nakayama, K. (2025). Promotion of bone-tendon healing after ACL reconstruction using scaffold-free constructs comprising ADSCs produced by a bio-3D printer in rabbit models. *Journal of Orthopaedic Translation*, *52*, 265-275.

[25] Li, Qiang, et al. "Inhibition of autophagy promoted high glucose/ROS-mediated apoptosis in ADSCs." Stem Cell Research & Therapy 9.1 (2018): 289.

[26] Liu, D., Liu, N., Liu, X., Liu, Y., Zhang, H., Zhou, Z., ... & Tian, Y. (2025). Adipose-derived stem cells (ADSCs)-derived DKK1 promotes cutaneous wound healing by inducing M2 macrophage polarization via PI3K/AKT and JNK activation. Biochimica et Biophysica Acta (BBA)-Molecular Cell Research, 120077.

[27] Chen, Y., Yin, W., Liu, Z., Lu, G., Zhang, X., Yang, J., ... & He, W. (2025). Exosomes derived from fibroblasts enhance skin wound angiogenesis by regulating HIF-1α/VEGF/VEGFR pathway. Burns & Trauma, 13, tkae071.

[28] Liu, H. M., Zhu, M., Wang, J., Luo, J. J., Ding, W., Ning, L. J., & Qin, T. W. (2025). Tendon-derived extracellular vesicles enhance TDSC activity and alleviate inflammatory response: a pathway to promote tendon regeneration. Journal of Materials Chemistry B, 13(46), 15024-15037.

Supplementary Files

This is a list of supplementary files associated with this preprint. Click to download.

- 12.bmp
- 13.bmp
- 14.bmp
- 15.bmp
- 110.bmp
- 16.bmp
- 17.bmp
- 18.bmp
- 19.bmp